Internal Transport Barrier Broadening through Subdominant Mode Stabilization in Reversed Field Pinch Plasmas

R. Lorenzini, F. Auriemma, A. Fassina, E. Martines, D. Terranova, and F. Sattin
Consorzio RFX, Corso Stati Uniti 4, I-35127 Padova, Italy

(Received 15 December 2015; revised manuscript received 25 February 2016; published 5 May 2016)

The reversed field pinch (RFP) device RFX-mod features strong internal transport barriers when the plasma accesses states with a single dominant helicity. Such transport barriers enclose a hot helical region with high confinement whose amplitude may vary from a tiny one to an amplitude encompassing an appreciable fraction of the available volume. The transition from narrow to wide thermal structures has been ascribed so far to the transport reduction that occurs when the dominant mode separatrix, which is a preferred location for the onset of stochastic field lines, disappears. In this Letter we show instead that the contribution from the separatrix disappearance, by itself, is marginal and the main role is instead played by the progressive stabilization of secondary modes. The position and the width of the stochastic boundary encompassing the thermal structures have been estimated by applying the concept of a 3D quasiseparatrix layer, developed in solar physics to treat reconnection phenomena without true separatrices and novel to toroidal laboratory plasmas. Considering the favorable scaling of secondary modes with the Lundquist number, these results open promising scenarios for RFP plasmas at temperatures higher than the presently achieved ones, where lower secondary modes and, consequently, larger thermal structures are expected. Furthermore, this first application of the quasiseparatrix layer to a toroidal plasma indicates that such a concept is ubiquitous in magnetic reconnection, independent of the system geometry under investigation.

DOI: 10.1103/PhysRevLett.116.185002

Introduction.—Magnetic field line reconnection, a process that converts magnetic field energy into kinetic and thermal energy, is at the heart of several phenomena in laboratory and astrophysical plasmas [1,2]. In the reversed field pinch (RFP) toroidal configuration for the confinement of fusion relevant plasmas [3], the same resonant tearing modes that self-sustain the configuration cause field line reconnection and make the magnetic field stochastic. However, the field stochasticity and the entailed anomalous transport are mitigated when the plasma accesses the quasisingle helicity state [4], where a single resonant mode dominates the spectrum of the secondary instabilities. In RFX-mod [5], the world's largest RFP experiment, quasisingle helicity plasmas feature steep electron temperature gradients, interpreted as internal transport barriers (ITBs) [6,7]. Such ITBs enclose helical thermal structures located inside the magnetic island of the dominant mode. A reduction of heat transport inside magnetic islands is observed also in tokamak and stellarator devices [8,9], and its active control is studied through the application of resonant magnetic perturbations [10]. In RFX-mod the spatial extent of thermal structures varies significantly; some of them are narrow and located off axis, while others are wide enough to enclose the geometrical axis. To date, such differences have been correlated to the topology of the magnetic field, determined by the combination of the axisymmetric equilibrium field with that due to the dominant mode. Specifically, earlier studies highlighted the major role played by the island separatrix, the magnetic surface that, in states with a double magnetic axis (DAx) [11], separates the surfaces nested around the main magnetic axis from those nested around the island O point. While narrow thermal structures feature a double axis with the separatrix, wide thermal structures occur when the dominant mode is large enough to make the separatrix disappear and the magnetic surfaces become nested around a single helical axis (SHAx) [12], the so-called saddle-node bifurcation. The explanation that was found is that the separatrix contains the X point, the magnetic null where field lines connect; since the X point favors the development of chaos generated by further perturbations, wider well confined regions are expected when the separatrix disappears [13]. In this Letter we show that the size of thermal structures is only marginally affected by the separatrix disappearance since it features a regular increasing trend with the dominant mode amplitude even across the DAx-SHAx transition. Moreover, there is a good correlation between the widening of thermal structures and the reduction of secondary mode amplitude, particularly that of the subdominant ones.

Our study benefits from three factors. First, the improvement of the helical force-free equilibrium field calculated with the SHEq code [14,15]. Indeed, while the calculation of the equilibrium was partially done in cylindrical geometry previously [12], the code now has been made fully self-consistent in toroidal geometry [16]. The difference in the magnetic quantities between the two calculations is small but not negligible. In fact, the improved reconstruction

accurately demonstrates that the kinetic pressure is a helical flux function [16,17] and allows the detailed characterization of the core magnetic field undergoing the saddle-node bifurcation [18]. A second important contribution is given by the collection of a large database of about 230 electron temperature T_e profiles featuring ITBs, measured along the machine horizontal diameter with a Thomson scattering diagnostic [19]. Such profiles were measured in quasisingle helicity plasmas, whose dominant helicity has the poloidal number $m = 1$ and the toroidal number $n = -7$. The third element of novelty is the interpretation of experimental data by means of the quasiseparatrix layer (QSL) concept, developed in solar physics to study magnetic reconnection phenomena without magnetic nulls [20], and adapted here to a toroidal geometry. The QSL is used to estimate quantitatively the size of the stochastic boundaries surrounding the ITBs. The conclusion of this study is that the process of thermal structure broadening, which results in an increase of the energy confinement time, is mainly driven by the stabilization of secondary modes. Since the secondary modes are stabilized by increasing the Lundquist number [21]—namely, increasing the temperature that in our Ohmic plasmas is approximately proportional to the plasma current—wider thermal structures and enhanced energy confinement are expected at higher currents. The above phenomenology shares many similarities with the results of heat transport control experiments performed in the Large Helical Device [22].

Analysis of thermal structure width.—The extent of the thermal structure is defined as the width W_{T_e} of the region where T_e exceeds by more than 30% the electron temperature averaged over the plasma internal region ($r \leq 0.35$ m) (Fig. 1). Figure 2(a) shows that W_{T_e} grows as the toroidal component of the dominant mode $b_T^{1,-7}$, measured at the edge and normalized to the edge magnetic field B_a, increases. However, there is a smooth transition between DAx states and SHAx states. This transition is located at roughly $b_T^{1,-7} = 1.5\%$; this value is lower by almost a threefold factor with respect to previous findings [12]. W_{T_e} increases steadily and about linearly up to $b_T^{1,-7} \sim 2.5\%$. From this point onwards, there is a moderate but evident change in slope up to $b_T^{1,-7} \sim 3.5\%$, while thermal structures remain located off axis. Above such a threshold [12], the barrier suddenly extends, encompassing both sides of the geometrical axis. The plot shows that thermal structures are off axis not only in DAx topologies but also in SHAx ones. The latter cases, which feature narrow structures in single helical axis states, will hereafter be called SHAx_n. Conversely, the cases with wide thermal structures, previously simply called SHAx [12], will hereafter be referred to as SHAx_w. The transition from narrow to wide thermal structures observed at $b_T^{1,-7} \sim 3.5\%$ cannot be ascribed to the transport mitigation induced by the saddle-node bifurcation, which occurs at lower $b_T^{1,-7}$, and calls for an additional chaos healing mechanism. If we plot the ensemble-averaged spectrum of secondary modes versus the dominant one [Fig. 2(b)], we observe a decrease of their amplitudes, especially for the two innermost resonant, subdominant modes $n = -8, -9$, when $b_T^{1,-7} > 2.5\%$; in particular, the $n = -8$ mode, which usually is the largest one, becomes comparable to the other modes with a higher toroidal number in the SHAx_w spectra. Moreover, the angular velocity of the two subdominant modes nearly doubles for SHAx_w with respect to the average value of

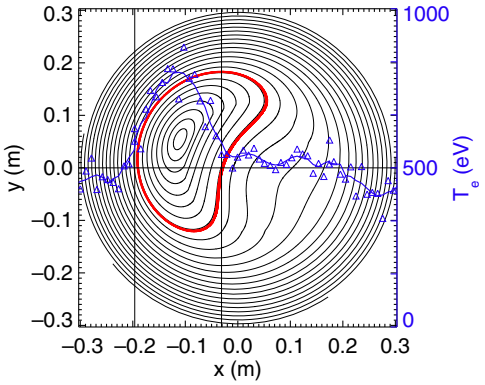

FIG. 1. Temperature profile (triangles) measured along a horizontal diameter, featuring a thermal structure overplotted to the magnetic surfaces. The vertical lines mark the structure width W_{T_e}. The red surface is S_{QSL}, defined in the text.

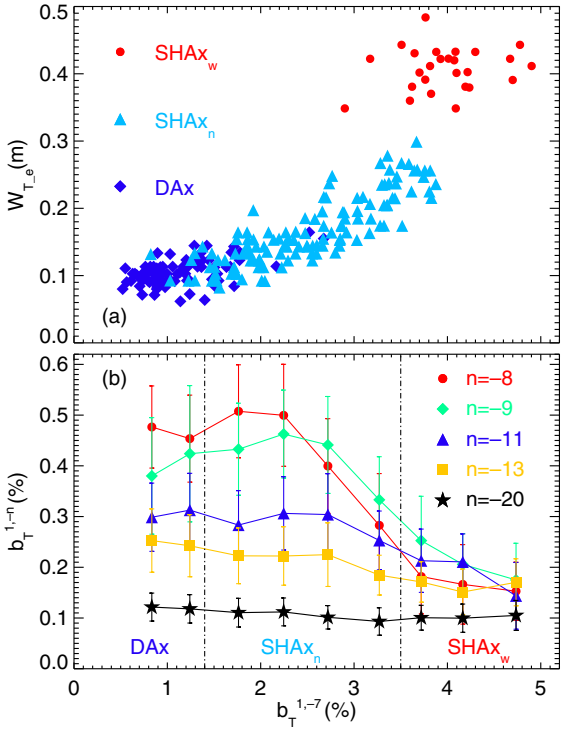

FIG. 2. (a) Thermal structure width W_{T_e} versus the dominant mode amplitude $b_T^{1,-7}$. (b) Ensemble-averaged amplitude of selected secondary modes versus $b_T^{1,-7}$.

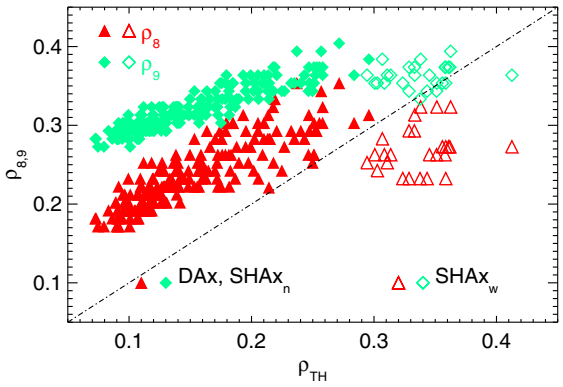

FIG. 3. Resonance positions of the $n = -8, -9$ modes, ρ_8 (red triangles) and ρ_9 (green diamonds), plotted versus the position ρ_{TH} of the ITB outermost points. Full symbols refer to DAx and SHAx_n states, whereas empty symbols pertain to SHAx_w states.

~70 Hz seen in DAx and SHAx_n plasmas. Since the island width is proportional to the mode amplitude and is inversely proportional to the angular velocity [23], the above analysis indicates that SHAx_w plasmas feature the smallest $n = -8, -9$ islands. This in turn suggests that SHAx_w structures might occur when the reduced overlapping of $n = -8, -9$ mode islands mitigates the field stochasticity between the two resonance radii. This hypothesis is supported by Fig. 3, where the positions of ITB outermost points (ρ_{TH}) are compared with the positions ρ_8 and ρ_9 of the $n = -8, -9$ mode resonances, according to the safety factor q of the helical equilibrium calculated as in Ref. [24]. Since q and T_e are helical flux functions, the helical radial coordinate ρ [14] is used. It is seen that both resonances are external to DAx and SHAx_n structures ($\rho_{8,9} > \rho_{\mathrm{TH}}$), suggesting that in such plasmas the island overlap induces a strong stochasticity that prevents the formation of thermal gradients between ρ_8 and ρ_9. Conversely, SHAx_w structures include ρ_8, so that the ITB gradients lie between the two resonances ($\rho_8 < \rho_{\mathrm{TH}} < \rho_9$). This implies that, in the latter case, the stochasticity is mitigated due to the smaller island size.

Implementation of the QSL model.—As shown in the previous section, narrow thermal structures steadily enlarge as $b_T^{1,-7}$ increases. Such a dependence, and the minor role played in such a process by the X point disappearance, suggests that the vulnerability to magnetic chaos is related to a more global property of the magnetic topology. Our aim is to define such a property, through a model that also includes the variation of magnetic perturbations shown in Fig. 2(b). Since most of the narrow thermal structures are observed when the separatrix is absent, we took inspiration from the effort done by the solar physics community to explain the occurrence of solar flares in the absence of magnetic nulls [25]. The concept of separatrix has been generalized in 3D configurations to quasiseparatrix layers, defined as regions where there is a continuous, significant change of field line linkage [26]; if a separatrix exists it is part of the QSL as a particular case of discontinuous field line linkage. Considering the lines that connect photospheric areas of positive and negative magnetic polarities through a map $\mathbf{r}_+ \mapsto \mathbf{r}_-$, a QSL is found where such a mapping results in a squashing of the flux tube cross sections, for example, when a tiny circular region is mapped to a very elongated elliptical region. In analogy to solar physics, we assume that in our plasma quasiseparatrix layers behave physically like separatrices; the squashing of flux tubes becomes the global property that plays the role of seed for the chaos induced by magnetic perturbations. The most used indicator to identify a QSL is the squashing degree Q [27,28], a pure number proportional to the norm of the Jacobian matrix of the map. A QSL is found where Q exceeds a threshold, whose value is typically based on the Q profile itself, defining, for example, the QSL width as the full width at half maximum of the Q profile [29]. While solar physics and a previous QSL application to laboratory plasmas [30] address a line-tied problem, in a toroidal system a field line covers ergodically its magnetic surface and has infinite foot points on a poloidal plane. This prevents the use of Q; therefore, we defined a more suitable indicator directly related to the flux tube squashing. The flux tube cross sections are the poloidal cross sections of the magnetic surfaces at the toroidal angle of the Thomson scattering diagnostic. Their squashing is defined through the dilatation that an infinitesimal area element dS, enclosed between two magnetic surfaces, undergoes when moving poloidally from a position where the surfaces are compressed to one where they are stretched. The surface dilatation is defined as the ratio between the "stretched" area dS_s and the "compressed" area dS_c, both taken under an arc of length dL [Fig. 4(a)].

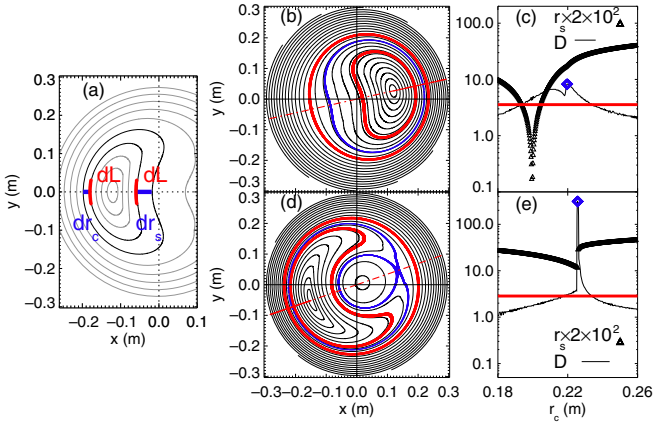

FIG. 4. (a) Depiction of variables used in Eq. (1). Magnetic surfaces of (b) a SHAx and (d) a DAx case. The red line is the collection diameter of r_c and r_s, the red full segment is the array of r_c values. The two red surfaces bound the QSL. (c),(e) r_s and D versus r_c. The horizontal red line indicates the $D = D_{\mathrm{th}}$ values of S_{QSL}, the innermost red surface of (b) and (d). The highest value of D (blue diamonds) identifies (b) the blue quasiseparatrix surface and (d) the separatrix.

Calling r_s and r_c the radial positions of dS_s and dS_c, respectively, the surface dilatation is

$$\frac{dS_s}{dS_c} \sim \frac{dL dr_s}{dL dr_c} = \frac{dr_s}{dr_c}. \quad (1)$$

The new indicator D is the surface dilatation, compensated for by the flux tube expansion due to the toroidal magnetic field as in Ref. [27]. Both r_s and r_c are collected along the diameter [Figs. 4(b) and 4(d)] that crosses the magnetic axis in SHAx states or the island O point in DAx states. Such a diameter intersects each magnetic surface twice: the r_c values are the radii of intersections found moving outwards from the magnetic axis, while the radii of intersections in the opposite direction give the r_s values. The chosen mapping $\mathbf{r}_c \mapsto \mathbf{r}_s$ is continuous in SHAx, while it is discontinuous in the DAx case at the separatrix [Figs. 4(c) and 4(e)], where D is the maximum. The SHAx surface having the highest D value may be seen as the remnant of the separatrix and will be called the quasiseparatrix surface. The QSL is the set of the most squashed surfaces, identified by the condition that D be higher than the threshold D_{th}; its innermost surface S_{QSL} encloses a set of weakly squashed surfaces, having $D < D_{\mathrm{th}}$. Under the hypothesis that the surface squashing favors the development of magnetic chaos, the QSL should correspond to the highly stochastic region surrounding magnetic surfaces more resilient to the magnetic chaos, which in turn host the thermal structures. Hence, the thermal structure width is estimated by computing the segment W_{QSL} of the Thomson scattering line of sight enclosed by S_{QSL}. To derive a threshold value for D related to the strength of the perturbations, D_{th} has been taken as inversely proportional to the width $\Delta_{1,-8}$ of the $n = -8$ mode magnetic island, which is closest to the thermal gradients:

$$D_{\mathrm{th}}{}^{-1} = A\sqrt{b_{r,\mathrm{res}}^{1,-8}} \propto \Delta_{1,-8}, \quad (2)$$

where $b_{r,\mathrm{res}}^{1,-8}$ is the radial field at the resonance radius and A is a constant whose value is fixed, matching W_{T_e} and W_{QSL} in a few reference SHAx$_n$ cases with $b_T^{1,-7} \sim 2\%$. In Figs. 4(b) and 4(d), the red lines identify the QSL region, which is located in the interface region among beanlike and circularlike magnetic surfaces. Figure 5(a) shows W_{QSL} versus $b_T^{1,-7}$ for the same database of narrow barriers as Fig. 2. The agreement between the experimental width and the calculated one is remarkable: in particularly similar W_{QSL} values are found for DAx and SHAx states with $b_T^{1,-7} \sim 1.5\%$. The dependence of the threshold on $b_{r,\mathrm{res}}^{1,-8}$ yields a nice fit to the increasing trend of W_{T_e}, reproducing even the slope change observed at $b_T^{1,-7} > 2.5\%$, although Fig. 5(b) shows that the model tends to underestimate the experimental widening. Another interesting result comes from the comparison of the quasiseparatrix helical coordinate ρ_{QS} with ρ_8 and ρ_{TH}. The ordering $\rho_8 > \rho_{\mathrm{QS}} > \rho_{\mathrm{TH}}$,

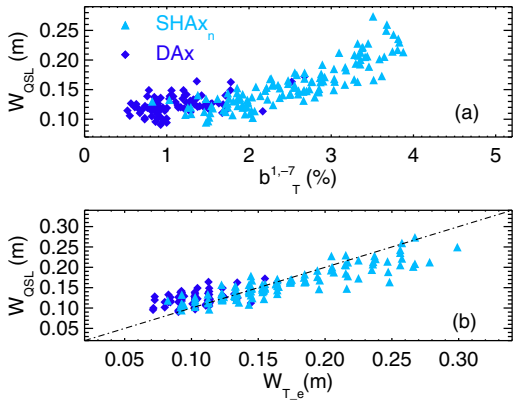

FIG. 5. W_{QSL} plotted (a) versus $b_T^{1,-7}$ and (b) versus W_{T_e}.

found in narrow thermal structures with low values of $b_T^{1,-7}$, modifies to $\rho_{\mathrm{TH}} > \rho_{\mathrm{QS}} > \rho_8$ in the case of SHAx$_w$. This means that the well confined region enclosed by the ITB of SHAx$_w$ structures expands beyond the region that hosts the stochastic QSL of narrow structures. Moreover, when the QSL model is applied to SHAx$_w$ cases, D_{th} is typically higher than the maximum value of D; hence, no stochastic QSL is found.

Conclusions.—This Letter shows that, in RFX-mod, the width of thermal structures enclosed by ITB features an increasing trend with the dominant mode amplitude. Such a trend is continuous and smooth even at the saddle-node bifurcation, and it is mainly driven by the stabilization of secondary modes. In particular, the confinement increase associated with the transition from SHAx$_n$ to SHAx$_w$ is due to the stabilization of the two subdominant modes. This result provides positive expectations for RFP plasmas with enhanced heating since, while it is difficult to envisage further bifurcations driven by the dominant mode, secondary modes are experimentally observed to be stabilized by increasing the Lundquist number, and their amplitude is theoretically predicted [31,32] to decrease with the plasma current. A deeper understanding of the above results is obtained by introducing the concept of quasiseparatrix layer, used to date to localize magnetic reconnection events, as the stochastic region that surrounds the thermal structures. This novel interpretation paves the way for the exploitation of the QSL concept in tokamaks and stellarators, providing a relatively simple method for estimating the stochastic layer width in experiments of transport control by resonant magnetic perturbations [22]. A further novel aspect of the QSL application presented here regards the link between the QSL threshold and a physical parameter having a relevant role in the process under examination. This choice, which provided a good match between experimental and model results, offers an alternative to the habit of determining the threshold from the topology itself. As a final remark, we emphasize that the above results validate the QSL model in a parameter space different from that in previous work. We extended the

concept to a toroidal free-boundary system, while previous applications were in line-tied geometry. Hence, this Letter demonstrates that the QSL is ubiquitous in three-dimensional magnetic reconnection.

The authors are indebted to S. Martini for the useful comments on the manuscript. This project received funding from the European Union Horizon 2020 research and innovation program under Grant Agreement No. 633053. The views and opinions expressed herein do not necessarily reflect those of European Commission.

[1] E. Priest and T. Forbes, *Magnetic Reconnection* (Cambridge University Press, Cambridge, England, 2000).
[2] E. G. Zweibel and M. Yamada, Annu. Rev. Astron. Astrophys. **47**, 291 (2009).
[3] S. Ortolani and D. D. Schnack, *Magnetohydrodynamics of Plasma Relaxation* (World Scientific, Singapore, 1993).
[4] D. F. Escande, P. Martin, S. Ortolani, A. Buffa, P. Franz, L. Marrelli, E. Martines, G. Spizzo, S. Cappello, A. Murari, R. Pasqualotto, and P. Zanca, Phys. Rev. Lett. **85**, 1662 (2000).
[5] P. Sonato *et al.*, Fusion Eng. Des. **66–68**, 161 (2003).
[6] M. Valisa *et al.*, Plasma Phys. Controlled Fusion **50**, 124031 (2008).
[7] R. Lorenzini *et al.*, Nucl. Fusion **52**, 062004 (2012).
[8] K. Ida, K. Kamiya, A. Isayama, and Y. Sakamoto (JT-60 Team), Phys. Rev. Lett. **109**, 065001 (2012).
[9] S. Inagaki, N. Tamura, K. Ida, Y. Nagayama, K. Kawahata, S. Sudo, T. Morisaki, K. Tanaka, T. Tokuzawa, and LHD Experimental Group, Phys. Rev. Lett. **92**, 055002 (2004).
[10] K. Ida, T. Kobayashi, T. E. Evans, S. Inagaki, M. E. Austin, M. W. Shafer, S. Ohdachi, Y. Suzuki, S.-I. Itoh, and K. Itoh, Sci. Rep. **5**, 16165 (2015).
[11] M. E. Puiatti *et al.*, Plasma Phys. Controlled Fusion **51**, 124031 (2009).
[12] R. Lorenzini, D. Terranova, A. Alfier, P. Innocente, E. Martines, R. Pasqualotto, and P. Zanca, Phys. Rev. Lett. **101**, 025005 (2008).
[13] D. F. Escande, R. Paccagnella, S. Cappello, C. Marchetto, and F. D'Angelo, Phys. Rev. Lett. **85**, 3169 (2000).
[14] E. Martines *et al.*, Plasma Phys. Controlled Fusion **53**, 035015 (2011).
[15] P. Zanca and D. Terranova, Plasma Phys. Controlled Fusion **46**, 1115 (2004).
[16] R. Lorenzini *et al.*, Nat. Phys. **5**, 570 (2009).
[17] F. Auriemma *et al.*, Plasma Phys. Controlled Fusion **53**, 105006 (2011).
[18] W. F. Bergerson, F. Auriemma, B. E. Chapman, W. X. Ding, P. Zanca, D. L. Brower, P. Innocente, L. Lin, R. Lorenzini, E. Martines, B. Momo, J. S. Sarff, and D. Terranova, Phys. Rev. Lett. **107**, 255001 (2011).
[19] A. Alfier and R. Pasqualotto, Rev. Sci. Instrum. **78**, 013505 (2007).
[20] P. Démoulin, Adv. Space Res. **37**, 1269 (2006).
[21] P. Piovesan *et al.*, Nucl. Fusion **49**, 085036 (2009).
[22] K. Ida. S. Inagaki, Y. Suzuki, S. Sakakibara, T. Kobayashi, K. Itoh, H. Tsuchiya, C. Suzuki, M. Yoshinuma, Y. Narushima, M. Yokoyama, A. Shimizu, S-I. Itoh, and LHD Experiment Group, New J. Phys. **15**, 013061 (2013).
[23] R. Fitzpatrick, S. C. Guo, D. J. Den Hartog, and C. C. Hegna, Phys. Plasmas **6**, 3878 (1999).
[24] B. Momo, E. Martines, D. F. Escande, and M. Gobbin, Plasma Phys. Controlled Fusion **53**, 125004 (2011).
[25] P. Démoulin, J. C. Hénoux, and C. H. Mandrini, Astron. Astrophys. **285**, 1023 (1994).
[26] P. Démoulin, E. R. Priest, and D. P. Lonie, J. Geophys. Res. **101**, 7631 (1996).
[27] V. S. Titov, G. Hornig, and P. Démoulin, J. Geophys. Res. **107**, SSH 3-1 (2002).
[28] J. M. Finn, Z. Billey, W. Daughton, and E. Zweibel, Plasma Phys. Controlled Fusion **56**, 064013 (2014).
[29] G. Aulanier, E. Pariat, and P. Démoulin, Astron. Astrophys. **444**, 961 (2005).
[30] E. E. Lawrence and W. Gekelman, Phys. Rev. Lett. **103**, 105002 (2009).
[31] J. H. Kim and P. W. Terry, Phys. Plasmas **19**, 122304 (2012).
[32] P. W. Terry and G. G. Whelan, Plasma Phys. Controlled Fusion **56**, 094002 (2014).